A Kinetic Investigation of High-Temperature Mercury Oxidation by Chlorine

Jennifer Wilcox†

Department of Energy Resources Engineering, Stanford University, 367 Panama Street, Stanford, California 94305.

Received: February 4, 2009; Revised Manuscript Received: April 23, 2009

First-stage mercury oxidation reactions typical of coal combustion flue gases were investigated. The present study is a determination of the kinetic and thermodynamic parameters of the bimolecular reactions, Hg + Cl_2 ↔ HgCl + Cl, Hg + HCl ↔ HgCl + H, and Hg + HOCl ↔ HgCl + OH, at the B3LYP/RCEP60 VDZ level of theory over a temperature range of 298.15 to 2000 K at atmospheric pressure. Conventional transition state theory was used to predict the forward and reverse rate constants for each reaction and ab initio based equilibrium constant expressions were calculated as a function of temperature. Reasonable agreement was achieved between the calculated equilibrium constants and the available experimental values.

Introduction

Coal as the most abundant fossil fuel on the planet is sufficient to meet current energy demand for nearly 200 years with approximately 900 billion metric tons available.[1] To meet the growing world energy demand, which is driven primarily by developing countries such as China and India, dependence on fossil fuels will remain prominent likely into the first half of the 21st century. Coal-based power plants currently generate approximately 50% of the electricity for the United States.[2] A typical 500 MW power station will consume 6000 tons per day of coal.[3] Currently the U.S. has the equivalent of >500 full-scale (500 MW) coal-fired power plants with an average age of 35 years.[4] Coal-fired power plants are the greatest anthropogenic source of mercury emissions in the United States. Power generation is responsible for 37% of the mercury released into the environment from human activity, with about 48 tons per year released in the United States.[5] Attempts have been made to model homogeneous mercury oxidation in the flue gas environment through reaction channels involving chlorine explicitly.[6−8] Experimentally and theoretically derived rate data available in the literature for modeling mercury−chlorine reactions at combustion conditions are limited.

Applications of previous kinetic investigations on halogen-oxidized mercury species have primarily dealt with the cycling of mercury within the atmosphere. Although the previous studies are very thorough, they do not give an indication of mercury oxidation behavior at the high-temperature conditions of coal combustion. In particular there have been five experimental[9−13] and four theoretical[14−17] accounts of mercury oxidation via chlorine species. These studies focus primarily on the oxidation of mercury via chlorine radicals, which is the primary mechanism for mercury oxidation via chlorine species under atmospheric conditions. The lack of agreement among the experimental kinetic investigations highlights the difficulty associated with measuring the highly reactive oxidized mercury species. Details of these previous investigations will not be included here, but Donohoue et al. have given a nice review of several of these in a recent publication.[10] The investigation of Donohoue et al. may provide the most accurate rate prediction of the association of mercury with chlorine atom since they are the first group to systematically vary the temperature, pressure, and buffer gases and found that the observed behavior was consistent with the behavior expected for a three-body recombination. Understanding the first stage of mercury oxidation via chlorine species is the first step in understanding its complete speciation. Unique from the lower temperatures of the marine boundary layer, the coal combustion-generated flue gas spans a broad temperature range, from the high temperature of the boiler region to the low outlet temperature of the stack. Within this quench zone mercury oxidation requires a complex series of homogeneous and heterogeneous interactions. The heterogeneous chemistry is driven by a combination of systems that is unique to a given utility boiler, e.g., unburned carbon, fly ash, and catalytic surfaces of selectively catalytic reducing systems and sulfur dioxide scrubbing systems. It is commonly thought that the homogeneous chemistry is primarily chlorine-driven. Quantifying the extent of homogeneous oxidation will allow for global combustion models to more accurately predict the extent of heterogeneous oxidation, which will allow utility boilers to determine how to retrofit their existing systems to ultimately maximize their mercury capture. The current study is the first attempt to determine the kinetics of the first-stage mercury oxidation via HCl, Cl_2, or HOCl. Although the role of these species may be minimal for mercury oxidation under atmospheric conditions, their role is critical in understanding mercury's speciation in the quench zone of flue gases. Understanding the kinetic and thermodynamic behavior of mercury from the high to low temperature regime will allow for increased model accuracy in predicting mercury's complicated speciation, which in turn will facilitate the design and application of more effective mercury control devices.

In an attempt to provide current models with a more complete kinetic data set, rate expressions for the following reactions predicted through ab initio molecular orbital calculations are discussed within this work:

$$\mathrm{Hg} + \mathrm{HCl} \underset{k_{-1}}{\overset{k_1}{\longleftrightarrow}} \mathrm{HgCl} + \mathrm{H} \qquad (1)$$

† Phone: 650-724-9449. E-mail: wilcoxj@stanford.edu.

10.1021/jp901050d CCC: $40.75
Published on Web 05/26/2009

$$Hg + Cl_2 \underset{k_{-2}}{\overset{k_2}{\leftrightarrow}} HgCl + Cl \quad (2)$$

$$Hg + HOCl \underset{k_{-3}}{\overset{k_3}{\leftrightarrow}} HgCl + OH \quad (3)$$

To develop a more complete understanding of the overall speciation it is thus necessary to determine the importance of these compounds. To accomplish this, computational chemistry techniques are employed to determine the kinetic parameters of the elementary reactions taking place within the combustion flue gas environment.

Since these reactions are both single displacement reactions, transition state theory (TST) was used to determine the kinetic parameters of forward and reverse reactions for a temperature range of 298.15−2000 K at atmospheric pressure.

Computational Methodology. Calculations were carried out with the Gaussian03 suite of programs.[18] Basis sets incorporating relativistic effects for the inner electrons were employed through the use of small core relativistic effective core potentials (ECP) for these electrons. The basis set used in the potential energy surface investigations for mercury employs a relativistic compact effective potential, RCEP60 VDZ of the Stevens et al. group,[19] which replaces 60 of mercury's atomic core electrons, derived from numerical Dirac−Fock wave functions by using an optimizing process based upon the energy-overlap functional. Energy-optimized (8s8p5d)/[4s4p3d] Gaussian-type double-ς quality sp and triple-ς quality d functions were used for mercury, with the triple-ς quality d functions essential for describing the orbital shape changes that exist with d occupancy. An extended triple-ς quality Pople basis set, 6-311++G(3pd,3df), including both diffuse and polarization functions was used for oxygen, chlorine, and hydrogen atoms.

Justification for Method and Basis Set Selection. Before the kinetic and equilibrium parameters could be calculated, it was necessary to determine which level of theory would be the most accurate for the mercury compounds. From Table 1 it can be seen that the B3LYP/RCEP60 VDZ level of theory predicts bond distances, vibrational frequencies, and thermochemical data of the reaction species quite well, deviating minimally from experimental data available in the literature. The theoretical predictions of the current work were compared to experimental[20−23] and high-level theoretical[15,16,18] calculations available in the literature.

There have been many experimental and theoretical calculations performed on the determination of the HgCl and $HgCl_2$ equilibrium bond distances. Experimental measurements[22−25] of the HgCl bond distance range from 2.36 to 2.50 Å. Using the density functional method B3LYP with the relativistic effective core potential RCEP60 VDZ predicts a distance of 2.4896 Å, which falls within the experimental measurements. Khalizov et al.[15] reported a similar value, i.e., 2.398 Å, at the higher correlated level, QCISD, employing a similar basis set as the current study. The experimental bond distances[24−26] for $HgCl_2$ range from 2.25 to 2.44 Å. Using the B3LYP/RCEP60 VDZ level of theory predicts a distance of 2.3198 Å, which is well within the range of experiment. Balabanov and Peterson[16] carried out calculations using the high-level correlated CCSD(T) method along with an extensive basis set, which allowed the energy to be extrapolated to the CBS limit. The energy extrapolation to the CBS limit results in a shortening of the bond distance yielding a prediction of 2.2483 Å.

The predicted vibrational frequencies of the ground states of HgCl and $HgCl_2$ have also been compared to experimental and high-level theoretical predictions available in the literature. There have been two reports of experimental vibrational frequencies for HgCl in the literature, i.e., 292.6[27] and 298.97[28] cm^{-1}. At the B3LYP/RCEP60 VDZ level of theory, the predicted vibrational frequency is 244.40 cm^{-1}, within 50 wavenumbers of the experimental data. This same level of theory predicted the $HgCl_2$ vibrational frequencies with higher accuracy. The

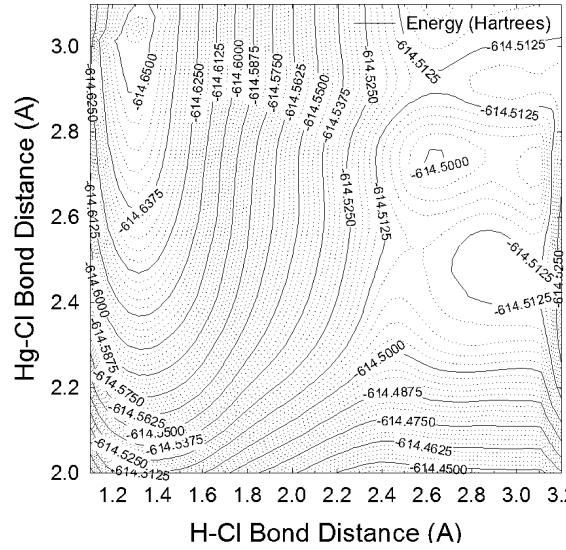

Figure 1. Hg + HCl ↔ HgCl + H: linear transition structure (B3LYP/RCEP60 VDZ).

TABLE 1: Theory Selection Criteria Comparison

	Hg−Cl		Hg−Cl_2	
parameter	B3LYP/RCEP60 VDZ	exptl	B3LYP/RCEP60 VDZ	exptl
bond length (Å)	2.4896	2.36−2.50[a]	2.3198	2.25−2.44[b]
bond angle (deg)	180	180	180	180
vib freq (cm^{-1})	244.40	292.6[c]	92 (Π_u)	100 (Π_u)[e]
		298.97[d]	318 (Σ_g)	313, 355, 358, 360, 365, 366 (Σ_g)[f]
			374 (Π_u)	376,[g] 413(Π_u)[h]

	$\Delta_r H_{298.15K}$ (kcal/mol)		
	reaction *1*	reaction *2*	reaction *3*
B3LYP/RCEP60 VDZ	79.009	31.797	29.649
exptl	78.243[i]	33.071[j]	31.209[i]

[a] References 22−25. [b] Reference 25−27. [c] Reference 28. [d] Reference 29. [e] Reference 30. [f] Reference 31 and 32. [g] Reference 32. [h] Reference 33. [i] Reference 29. [j] Reference 34.

doubly degenerate Π_u state has a reported experimental vibrational frequency of 100[29] cm^{-1} with the prediction lying within 10 wavenumbers at 92 cm^{-1}. Experimentally, the Σ_g state has been difficult to measure and many reports of this value are available in the literature, ranging from 313[30] to 366[31] cm^{-1}. The current prediction at the B3LYP/RCEP60 VDZ level of theory falls within this range at 318 cm^{-1}. Finally, the Σ_g state has also been reported with values ranging from 376[32] to 413[32] cm^{-1}, with the B3LYP/RCEP60 VDZ level of theory prediction deviating minimally at 374 cm^{-1}.

In addition to the geometry and spectroscopic predictions, the thermochemistry of reactions 1 through 3 has also been examined and compared to experiment where available. Of reactions 1 through 3, only the enthalpy of reaction 2 has been reported in the literature. The experimental value has been reported as 32.89 ± 2.29 kcal/mol at 298.15 K.[33] The B3LYP/RCEP60 VDZ level of theory predicts a value of 31.797 kcal/mol, which lies well within the experimental range. Balabanov and Peterson,[16] using high-level ab initio calculations, report an enthalpy of reaction at the same conditions of 35.1 kcal/mol. They performed their calculations at the CCSD(T) level of theory, including zero-point energy, core−valence correlation, pseudopotential corrections, scalar relativity, and spin−orbit coupling contributions with CBS-extrapolated basis sets in their computational methodology. The current work includes only the zero-point contribution to total energies, and neglects these additional corrections.[15] The ultimate goal of the current work is to generate rate expressions for inclusion into combustion models to accurately predict the speciation of mercury through a simulated quenching flue gas. To the author's knowledge, reaction enthalpies for reactions 1 and 3 have not been reported in the literature, but were calculated from reported formation enthalpies[29] of the individual reactant and product species. At the B3LYP/RCEP60 VDZ level of theory the predicted reaction enthalpy for reaction 1 was 79.009 kcal/mol compared to an experimental value of 78.243 kcal/mol and for reaction 3, the prediction was 29.649 kcal/mol compared to an experimental value of 31.209 kcal/mol. In total, a balance of computational cost and accuracy was achieved at the B3LYP/RCEP60 VDZ level of theory for reactions 1 through 3 and from the theory validation, extensive potential energy surfaces have been generated and corresponding rate expressions determined.

Theoretical Kinetic Methodology. Kinetic and equilibrium parameters were evaluated over a temperature range spanning 298.15−2000 K. In determining the rate constant for each reaction, the transition state theory[34] eq 4 was modified with the tunneling correction factor of Wigner[35] (eq 5) (where ν represents the single imaginary frequency value of the transition structure), so that the final rate constant value is given by eq 6. When the reaction coordinate is dominated by the motion of a hydrogen atom, correction for tunneling is crucial. For reactions 1 through 3, the reaction coordinate is dominated by the bond forming between a chlorine and mercury atom. For this reason, the simplest, Wigner correction is used to account for tunneling.

$$k^{TST} = \frac{k_b T}{h}\frac{Q_{TS}}{Q_1 Q_2} e^{(-E_a/RT)} \quad (4)$$

$$k_T = 1 + \frac{1}{24}\left[\frac{hc\nu}{k_b T}\right]^2 \quad (5)$$

$$k = k^{TST} k_T \quad (6)$$

In eqs 4, 5, and 6, k_b is Boltzmann's constant, h is Plank's constant, T is temperature, E_a is the activation barrier, R is the ideal gas constant, and Q_{TS}, Q_1, and Q_2 are the total partition functions of the transition structure and reaction species 1 and 2, respectively.

Additionally, the equilibrium constants for each reaction were calculated from eqs 7 and 8. By determining the thermodynamic parameters of reaction enthalpy and entropy, the equilibrium curve as predicted both theoretically and experimentally could be compared, where all data existed.

$$K_{eq} = e^{(-\Delta G/RT)} \quad (7)$$

$$\Delta G_{rxn} = \Delta H_{rxn} - T\Delta S_{rxn} \quad (8)$$

Results and Discussion

Potential energy surfaces were generated for reactions 1 through 3 and are shown in Figures 13, respectively. Each surface was generated with approximately 150 single-point energy calculations at the B3LYP/RCEP60 VDZ level of theory. Zero-point-inclusive thermochemical corrections to energy were not included in each single-point energy calculation, but were added to the subsequent transition state, reactant, and product energies for the activation barrier predictions. Density functional theory (DFT) was chosen due to its speed and relative accuracy in geometry, vibrational frequency, and thermochemical predictions compared to experiment, as highlighted in Table 1. One discrepancy that deserves attention is the difference between the predicted and experimental vibrational frequency of the HgCl radical. DFT underpredicts the experimental value by 48 cm^{-1}. A sensitivity analysis was performed on the rate constant calculations and it was found that this difference in HgCl vibration changes the rate constant by less than 2%. Also, DFT has shown to exhibit minimal spin contamination with unrestricted DFT.[36] Unrestricted DFT was employed for all open-shell systems, which include the activated complexes for each

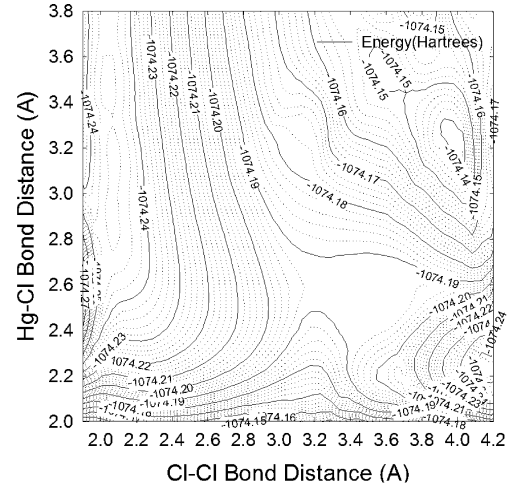

Figure 2. Hg + Cl_2 ↔ HgCl + Cl: linear transition structure (B3LYP/RCEP60 VDZ).

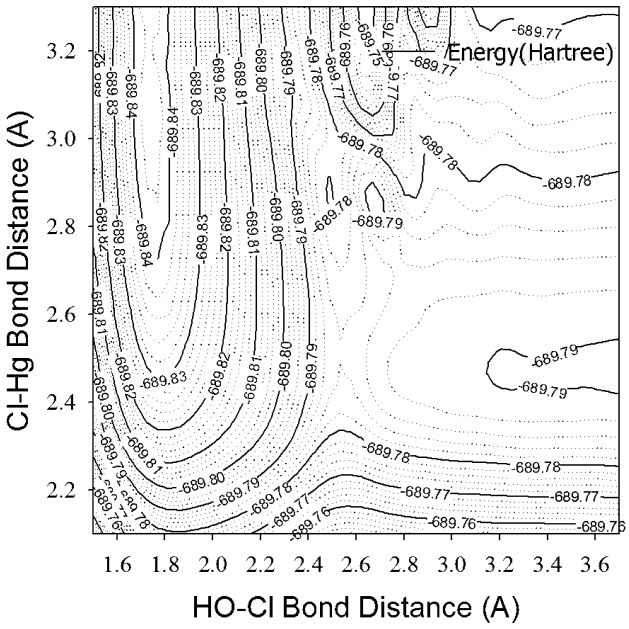

Figure 3. Hg + HOCl ↔ HgCl + OH: linear transition structure (B3LYP/ RCEP60 VDZ).

TABLE 2: Transition Structure Parameters

	$Hg^{1}-Cl^{2}-H$	$Hg^{1}-Cl^{2}-Cl$	$HO^{1}-Cl^{2}-Hg$
Bond 1 Length (Å)	2.55	2.55	2.50
Bond 2 Length (Å)	2.7	3.45	2.51
Bond 2 Angle (°)	180.0	180.0	∠*OClHg* 180.0 ∠*HOCl* 102.5
Vibrational Frequencies (cm^{-1})	206.654	92.141	128.551
	419.573	92.141	140.109
	419.573	170.108	190.891
	678.447*i*	109.497*i*	569.900
			3893.85
			195.619*i*
Single Point Energy (Hartrees)	-614.504	-1074.18	-689.785
Spin Multiplicity	1	1	1
Rotational Constant (GHZ)	2.32184	0.43661	611.232
			0.783
			0.782
I_{xx} (amu·Å^2)	0	0	0.868
I_{yy} (amu·Å^2)	4610.95	3760.61	532.291
I_{zz} (amu·Å^2)	0	0	533.159

of the three reactions examined. The calculated square of total spin is quite close to its eigenvalues s (s + 1), indicating that the spin contamination is minor. For each of the open-shell species, OH, HgCl, and Cl, the deviation from $\langle S^2 \rangle$ is 0.0026, 0.0048, and 0.0031, respectively. For H and each of the three activated transition complexes, the deviation is zero.

The electronic transition from the s^2 ground state to the first excited state, s^1p^1, was calculated as 5.11 eV at the B3LYP/ RCEP60 VDZ level of theory. The available thermal energy at the maximum conditions considered, i.e., 2000 K, is 0.172 eV, which is clearly not sufficient to produce this first excited state. Therefore, the s^2 ground state of Hg^0 was considered in all the calculations.

Forward rate expressions are depicted graphically in Figure 4. The natural log of the rate constant as a function of inverse temperature is graphed along with error bars for each kinetic prediction. The error bars were calculated by using a deviation of the model activation energy from the calculated activation barrier at each temperature, from 298.15 to 2000 K. The details of each oxidation channel are discussed individually.

A. Mercury Oxidation via HCl. A potential energy surface for reaction 1 is shown in Figure 1. A linear transition structure was assumed for the triatomic activated complex, H−Cl−Hg. An H−Cl distance of 2.70 Å and a Cl−Hg distance of 2.55 Å were found to possess the one imaginary frequency indicative of a transition structure with the relevant parameters of the structure given in Table 2. Having identified the transition structure for this reaction, the kinetic rate parameters were then investigated by using traditional transition state theory. The natural log of the forward rate constant (cm^3/(mol·s)) as a function of the inverse of temperature (K) is plotted in Figure

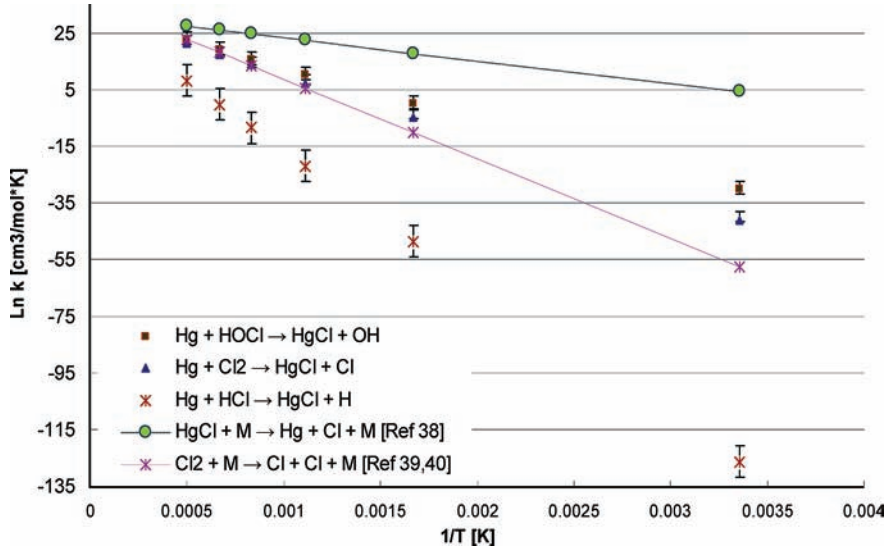

Figure 4. Comparison of forward rate constants as a function of temperature.

TABLE 3: Kinetic and Thermodynamic Parameters (Hg + HCl (k_1) ↔ (k_{-1}) HgCl + H)

	temperature (K)					
parameter	298.15	600	900	1200	1500	2000
K_{eq}(Th)	8.10×10^{-58}	1.33×10^{-28}	6.52×10^{-19}	4.87×10^{-14}	4.22×10^{-11}	3.76×10^{-8}
K_{eq}(Exp)	2.00×10^{-57}	1.76×10^{-28}	6.98×10^{-19}	4.72×10^{-14}	3.87×10^{-11}	3.29×10^{-8}

TABLE 4: Kinetic and Thermodynamic Parameters (Hg + Cl_2 (k_2) ↔ (k_{-2}) HgCl + Cl)

	temperature (K)					
parameter	298.15	600	900	1200	1500	2000
K_{eq}(Th)	8.49×10^{-23}	4.72×10^{-11}	3.55×10^{-7}	3.09×10^{-5}	4.52×10^{-4}	6.61×10^{-3}
K_{eq}(Exp)	1.46×10^{-23}	2.53×10^{-11}	2.88×10^{-7}	3.14×10^{-5}	5.31×10^{-4}	9.10×10^{-3}

4. Evaluating the trendlines associated with each method shows that, over the given temperature range, the Arrhenius expressions are

$$k_f^{TST} = 1.93 \times 10^{13} \exp\left(-\frac{93.3}{RT}\right) (\text{cm}^3/(\text{mol}\cdot\text{s})) \quad (9)$$

$$k_r^{TST} = 2.55 \times 10^{12} \exp\left(-\frac{13.8}{RT}\right) (\text{cm}^3/(\text{mol}\cdot\text{s})) \quad (10)$$

The activation energies used in the rate constant equations were compared to the exact values at each temperature and it was found that the forward reaction activation energy of 93.3 kcal/mol deviated by no more than approximately 3 kcal/mol while the reverse reaction value of 13.8 kcal/mol deviated at most by 2.5 kcal/mol. The highest deviations were found at the lower temperatures examined, suggesting that the deviation from the developed model will increase as temperature decreases.

B. Mercury Oxidation via Cl_2. The same basic procedure was followed in the determination of the kinetic parameters of reaction 2 with the potential energy surface plotted in Figure 2. The saddle point is clearly illustrated and the approximate coordinates (2.55 Å, 3.45 Å) proved to be a true transition structure with a single imaginary frequency, as before the parameters of which are shown in Table 2. The natural log of the forward rate constant ($cm^3/(mol\cdot s)$) as a function of the inverse of temperature (K) is plotted in Figure 4. Evaluating the trendlines associated with each method shows that, over the given temperature range, the Arrhenius expressions are

$$k_f^{TST} = 6.15 \times 10^{13} \exp\left(-\frac{43.3}{RT}\right) (\text{cm}^3/(\text{mol}\cdot\text{s})) \quad (11)$$

$$k_r^{TST} = 7.23 \times 10^{12} \exp\left(-\frac{11.8}{RT}\right) (\text{cm}^3/(\text{mol}\cdot\text{s})) \quad (12)$$

A comparison of the TST activation energies to exact values calculated at each temperature shows that the forward reaction value of 43.3 kcal/mol deviated by at most 1.7 kcal/mol while the reverse reaction value of 11.8 kcal/mol deviated by at most 1.9 kcal/mol, both reaching the maximum deviation at 298.15 K.

C. Mercury Oxidation via HOCl. The potential energy surface (PES) allows for a possible four degrees of freedom. To generate a 3-D plot, it was assumed based upon the gas-phase distances of OH and O−H within HOCl that the O−H distance changes minimally throughout the reaction and that the reaction proceeds at an angle of 102.5°, which is the gas-phase bond angle of the HOCl molecule. The experimental bond distance for the gas-phase OH molecule is 0.96966 Å and that for the O−H distance in the HOCl molecule 0.975 Å.[37] The two variables examined were the bond distances for the Hg−Cl and Cl−OH bonds. The potential energy surface is shown in Figure 3 in which the point on the graph shows a saddle point, indicative of the correct parameters of a transition structure, at approximately (2.50 Å, 2.51 Å). The harmonic frequency for the internal rotation of hydrogen in the transition structure for this reaction was found to be relatively high, i.e., 569.90 cm^{-1}. As the Hg−Cl bond is forming along the reaction coordinate, the Cl−O bond is breaking and the H atom is rotating freely out of the plane. Due to the high nature of this vibrational mode, it was assumed that the treatment of this mode as a free rotor was not necessary and would not likely change the overall rate expression dramatically. Therefore all of the internal vibrational modes of the transition structure complex were treated as decoupled harmonic oscillators.

The kinetic parameters for the reaction were determined by using transition state theory and are available in Table 2. The natural log of the forward rate constant ($cm^3/(mol\cdot s)$) as a function of the inverse of temperature (K) is plotted in Figure 4. Evaluating the trendlines associated with each method shows that, over the given temperature range, the Arrhenius expressions are

$$k_f^{TST} = 3.06 \times 10^{13} \exp\left(\frac{-36.6}{RT}\right) (\text{cm}^3/(\text{mol}\cdot\text{s})) \quad (13)$$

$$k_r^{TST} = 6.87 \times 10^{11} \exp\left(\frac{-6.2}{RT}\right) (\text{cm}^3/(\text{mol}\cdot\text{s})) \quad (14)$$

Comparison of the TST activation energies to exact values calculated at each temperature shows that the forward reaction value of 36.6 kcal/mol deviated by at most 1.8 kcal/mol while the reverse reaction value of 6.2 kcal/mol deviated by at most 2 kcal/mol, both reaching the maximum deviation at 2000 K.

D. Data Comparison. A comparison of rate constants generated at the B3LYP/RCEP60 VDZ level of theory is provided in Figure 4. Over the entire temperature range of 298.15 to 2000 K, in general, oxidation involving HOCl is faster than that of Cl_2, which is faster than that of HCl. However, oxidation via HOCl and Cl_2 rival one another at high temperatures. The rate expressions for two additional reactions were plotted in Figure 4, i.e., HgCl + M ↔ Hg + Cl + M[38] and Cl_2 + M ↔ 2Cl + M.[39,40] Within each of these unimolecular reactions, M is the collision partner or gas bath, which does not participate chemically in the reactions, but is taken into account within the pressure-dependent kinetic predictions using RRKM theory. The depletion of HgCl as temperature decreases is faster than the three HgCl formation reactions, while

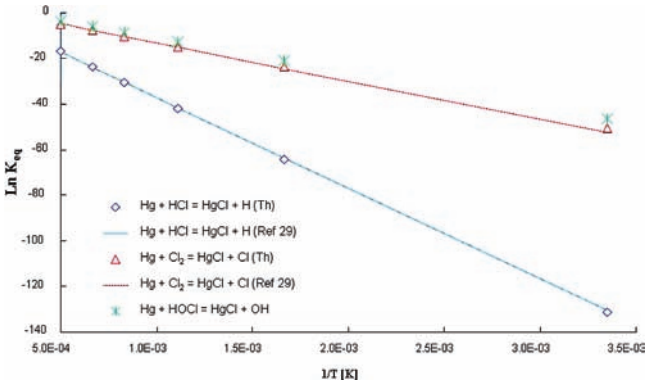

Figure 5. Equilibrium constant for reactions 1 through 3 as a function of temperature.

TABLE 5: Kinetic and Thermodynamic Parameters (Hg + HOCl (k_3) ↔ (k_{-3}) HgCl + OH)

	temperature (K)					
parameter	298.15	600	900	1200	1500	2000
K_{eq}(Th)	6.49^{-21}	6.39^{-10}	2.80^{-6}	1.84^{-4}	2.23^{-3}	2.66^{-2}
K_{eq}(Exp)						

comparable to the formation reactions involving HOCl and Cl_2 at high temperatures. The dissociation reaction of Cl_2 to chlorine radicals is comparable to the formation reactions involving HOCl and Cl_2 at high temperatures, but is slower at low temperatures, which ensures the presence of chlorine radicals at high temperatures. Due to the higher concentration of chlorine present in the flue gases compared to elemental mercury, the generation of chlorine radicals and the presence of Cl_2 should be expected throughout the quenching zone. This would imply that the oxidation reactions involving Cl and Cl_2 should be dominant over others and that oxidation involving HOCl will occur provided its concentration is available in sufficient quantity. However, it is important to note that this investigation is limited in that it is a comparison of a select group of mercury reactions. To accurately predict the complete pathway associated with homogeneous mercury oxidation, all of the reaction pathways will have to be compared, including those involving chlorine radicals, Cl_2, HCl, HOCl, in addition to submechanisms of chlorine and oxygen which will also influence mercury oxidation either directly or indirectly.

Additionally, the thermodynamic properties for each reaction were calculated from theory and compared to available experimental data[29] over a temperature range of 298.15 to 2000 K as seen in Tables 3−5 and graphically in Figure 5. The ab initio based thermochemical predictions are validated for reactions 1 and 2 as they agree with experiment quite well. Of the three reactions examined, the products of reaction 3 are the most thermodynamically favored over the temperature range. As temperature decreases, the equilibrium constant decreases for each reaction, which implies that the forward direction of each reaction is thermodynamically limited as temperature is decreased. Also, at lower temperatures, the oxidation of Hg via HCl is less likely than the other reaction channels.

Conclusions

This investigation provides additional thermochemical and kinetic insight into the first stage of mercury oxidation for coal combustion applications. Flue gas quenching is a crucial parameter for influencing mercury's speciation and its subsequent capture. Using density functional theory with a relativistic effective core potential for mercury with minimal energy corrections provided insight into the relative importance of the varying first-stage oxidation pathways of mercury. Both kinetic and thermodynamic predications indicate that of the three oxidizing species, Cl_2 and HOCl are more likely to play a major role in mercury's oxidation over HCl, but that atomic chlorine is likely involved in the dominant oxidation pathway. Future work will investigate a complete mechanism that will investigate the role of chlorine and oxygen submechanisms, which will help to elucidate the true potential of homogeneous mercury oxidation.

Acknowledgment. This material is based upon work supported by the National Science Foundation under Grant No. 0448758 and a WPI-based summer fellowship for undergraduate research. Recognition is given to Terumi Okano, Caitlin Callaghan, and Nicole Labbe for their assistance with the potential energy surface calculations. The authors would also like to thank Dr. Paul Blowers and Dr. Jost O. L. Wendt for their helpful discussions and for providing a starting point for these fruitful investigations.

References and Notes

(1) MIT Report, The Future of Coal, Options for a Carbon-Constrained World; MIT Press, 2007.
(2) Stewart, B. Coal Combustion Products (CCPs) Production and Use, 15th International Symposium On Management and Use of CCPs, Lexington, KY; American Coal Ash Assoc.: Aurora, CO, 2003; pp 20−22.
(3) Querol, X.; Fernandez-Turiel, J. L.; Lopez-Soler, A. *Fuel* **1995**, *74*, 331.
(4) U.S. Department of Energy, Energy Information Administration, International Outlook 2006, DOE/EIA-0484, 2006.
(5) Keating, M. H. Mercury study report to Congress. Volume II: Inventory of anthropogenic mercury emissions in the United States; U.S. Environmental Protection Agency, Office of Air Quality Planning and Standards, 1997.
(6) Sliger, R. N.; Kramlich, J. C.; Marinov, N. M. *Fuel Proc. Technol.* **2000**, *65*, 423.
(7) Niksa, S.; Fujiwara, N. *J. Air Waste Manage. Assoc.* **2005**, *55*, 930.
(8) Fry, A.; Cauch, B.; Silcox, G. D.; Lighty, J. S.; Senior, C. L. *Proc. Comb. Inst.* **2007**, *31*, 2855.
(9) Donohoue, D. L.; Bauer, D.; Hynes, A. J. *J. Phys. Chem. A* **2005**, *109*, 7732.
(10) Ariya, P. A.; Khalizov, A.; Gildas, A. *J. Phys. Chem. A* **2002**, *106*, 7310.
(11) Spicer, C. W.; Satola, J.; Abbgy, A. A.; Plastridge, R. A.; Cowen, K. A. Kinetics of Gas-Phase Elemental Mercury Reaction with Halogen Species, Ozone, and Nitrate Radical under Atmospheric Conditions; Florida Department of Environmental Protection, 2002.
(12) Taylor, P. H.; Mallipeddi, R.; Yamada, T. *Chemosphere* **2005**, *61*, 685.
(13) Horne, D. G.; Gosavi, R.; Strausz, O. P. *J. Phys. Chem.* **1968**, *48*, 4758.
(14) Khalizov, A. F.; Viswanathan, B.; Larregaray, P.; Ariya, P. A. *J. Phys. Chem. A* **2003**, *107*, 6360.
(15) Balabanov, N. B.; Peterson, K. A. *J. Chem. Phys.* **2003**, *119*, 12271.
(16) Wilcox, J.; Robles, J.; Marsden, D. C. J.; Blowers, P. *Environ. Sci. Technol.* **2003**, *37*, 4199–4202.
(17) Tossell, J. A. *J. Phys. Chem. A* **2003**, *107*, 7804.
(18) Frisch, M. J.; Trucks, G. W.; Schlegel, H. B.; Scuseria, G. E.; Robb, M. A.; Cheeseman, J. R.; Montgomery, J. A., Jr.; Vreven, T.; Kudin, K. N.; Burant, J. C.; Millam, J. M.; Iyengar, S. S.; Tomasi, J.; Barone, V.; Mennucci, B.; Cossi, M.; Scalmani, G.; Rega, N.; Petersson, G. A.; Nakatsuji, H.; Hada, M.; Ehara, M.; Toyota, K.; Fukuda, R.; Hasegawa, J.; Ishida, M.; Nakajima, T.; Honda, Y.; Kitao, O.; Nakai, H.; Klene, M.; Li, X.; Knox, J. E.; Hratchian, H. P.; Cross, J. B.; Bakken, V.; Adamo, C.; Jaramillo, J.; Gomperts, R.; Stratmann, R. E.; Yazyev, O.; Austin, A. J.; Cammi, R.; Pomelli, C.; Ochterski, J. W.; Ayala, P. Y.; Morokuma, K.; Voth, G. A.; Salvador, P.; Dannenberg, J. J.; Zakrzewski, V. G.; Dapprich, S.; Daniels, A. D.; Strain, M. C.; Farkas, O.; Malick, D. K.; Rabuck, A. D.; Raghavachari, K.; Foresman, J. B.; Ortiz, J. V.; Cui, Q.; Baboul, A. G.; Clifford, S.; Cioslowski, J.; Stefanov, B. B.; Liu, G.; Liashenko, A.; Piskorz, P.; Komaromi, I.; Martin, R. L.; Fox, D. J.; Keith, T.; Al-Laham, M. A.; Peng, C. Y.; Nanayakkara, A.; Challacombe, M.; Gill, P. M. W.; Johnson, B.; Chen, W.; Wong, M. W.; Gonzalez, C.; Pople, J. A. *Gaussian 03*, Revision C.02; Gaussian, Inc., Wallingford, CT, 2004.
(19) Stevens, W. J.; Krauss, M. *Can. J. Chem.* **1992**, *70*, 612.

(20) Liao, M. S.; Zhang, Q. E.; Schwarz, W. H. E. *Inorg. Chem.* **1995**, *34*, 5597.
(21) Schwerdtfeger, P.; Boyd, P. D. W.; Brienne, S.; McFeaters, J. S.; Dolg, M.; Liao, M. S.; Schwarz, W. H. E. *Inorg. Chim. Acta* **1993**, *213*, 233.
(22) Kaupp, M.; Vonschnering, H. G. *Inorg. Chem.* **1994**, *33*, 4179.
(23) Stroemberg, D.; Stroemberg, A.; Wahlgren, U. *Water, Air, Soil Pollut.* **1991**, *56*, 681.
(24) Cundari, T. R.; Yoshikawa, A. *J. Comput. Chem.* **1998**, *19*, 902.
(25) Kaupp, M.; Vonschnering, H. G. *Inorg. Chem.* **1994**, *33*, 2555.
(26) Stroemberg, D.; Gropen, O.; Wahlgren, U. *Chem. Phys.* **1989**, *133*, 207.
(27) Chase, M. W., Jr. NIST-JANAF Themochemical Tables, 4th ed. *J. Phys. Chem. Ref. Data* **1998**, Monograph 9.
(28) Tellinghuisen, J.; Tellinghuisen, P. C.; Davies, S. A.; Berwanger, P.; Viswanathan, K. S. *Appl. Phys. Lett.* **1982**, *41*, 789.
(29) Malt'sev, A. A.; Selivanov, G. K.; Yampolsky, V. I.; Zavalishin, N. I. *Nature, Phys. Sci.* **1971**, *231*, 157.
(30) Aylett, B. J. *Comprehensive Inorganic Chemistry*; Pergamon Press: Elmsford, NY, 1973; Vol. 3.
(31) Bell, S.; McKenzie, R. D.; Coon, J. B. *J. Mol. Spectrosc.* **1966**, *20*, 217.
(32) Adams, D. M.; Hills, D. J. *J. Chem. Soc., Dalton Trans.* **1978**, 776.
(33) Chase, M. W., Jr.; Davies, C. A.; Downey, J. R.; Frurip, D. J.; McDonald, R. A.; Syverud, A. N. *J. Phys. Chem. Ref. Data* **1985**, Monograph 14.
(34) Eyring, H. *J. Chem. Phys.* **1935**, *3*, 107.
(35) Wigner, E. *Z. Phys. Chem. Abt. B* **1932**, *19*, 203.
(36) Montoya, A.; Troung, T. N.; Sarofim, A. F. *J. Phys. Chem. A* **2000**, *104*, 6108.
(37) http://www.hbcpnetbase.com/; accessed April 9, 2009.
(38) Wilcox, J.; Marsden, D. C. J.; Blowers, P. *Fuel Proc. Technol.* **2004**, *85*, 391.
(39) Huybrechts, G.; Narmon, M.; Van Mele, B. *Int. J. Chem. Kinet.* **1996**, *28*, 27.
(40) Baulch, D. L.; Duxbury, J.; Grant, S. J.; Montague, D. C. *J. Phys. Chem. Ref. Data* **1981**, 10.

JP901050D